Available online at www.sciencedirect.com
SCIENCE DIRECT®
Journal of the European Ceramic Society 25 (2005) 1455–1462
www.elsevier.com/locate/jeurceramsoc

Structured porous Ni- and Co-YSZ cermets fabricated from directionally solidified eutectic composites

M.A. Laguna-Bercero, A. Larrea, J.I. Peña, R.I. Merino, V.M. Orera *

Instituto de Ciencia de Materiales de Aragón, C. S. I. C.—Universidad de Zaragoza, Pedro Cerbuna 12, 50009 Zaragoza, Spain

Accepted 14 April 2004
Available online 3 February 2005

Abstract

NiO-YSZ and CoO-YSZ eutectic rods were produced by directional solidification using the laser floating zone method (LFZ). This technique produces highly structured material consisting of alternate lamellae of transition metal oxide and zirconia with variable interlamellar spacing depending on growth conditions. We have chosen conditions for interlamellar spacing of about 1 μm. The microstructure is homogeneous and mechanically stable during thermochemical reduction. Complete reduction of the transition metal oxide produces a lamellar porous cermet with porous metallic lamellae alternated with the YSZ phase. The thermal expansion coefficients of the cermets are those of the YSZ skeleton. Reaction kinetics at different temperatures during the reduction process were studied by gravimetric methods. The reduction process within the complete temperature range studied for NiO-YSZ, and at high temperatures for CoO-YSZ seems to be controlled by the O^{2-} diffusion through the YSZ phase. The amount of Ni^{2+} and Co^{2+} ions dissolved in the YSZ phase is 2 and 5 mol%. Resistivity values for the cermets along the solidification axis are 50 μΩ cm for Co-YSZ and 130 μΩ cm for Ni-YSZ. These materials are porous, ionic and electronic conductors and could be used as textured anodes for solid-oxide fuel cells (SOFC).

Keywords: Directionally solidified eutectics; Composites; Electrical conductivity; Fuel cells

1. Introduction

Applications for porous cermets are found in many advanced areas of technology, including gas reactions and fuel cells. Solid-oxide fuel cells (SOFC) typically include a porous Ni-YSZ (yttria-stabilized zirconia) cermet anode and a tight YSZ thin layer as electrolyte. The cermet presents gas permeation and both, electronic and ionic conduction through metallic Ni and YSZ, respectively, thus increasing the density of triple phase boundary points (TPB) where the anode electrochemical reaction takes place. The microstructure of the anode and anode–electrolyte interface is a crucial issue to reduce the polarization loss of the cell.[1] Conventionally, Ni-YSZ cermets are produced by reduction of a NiO-YSZ ceramic to yield about 30–40% porosity as well as a good electronic and ionic conduction. Another suitable SOFC anode material is the Co-YSZ cermet.[2,3] The ceramic is prepared with fine and homogeneous powders to get as many TPB points as possible. However, grain coalescence at working temperatures (600–1000 °C) is a severe concern for the use of these ceramic electrodes. Lamellar electrodes produced by reduction of oxide–oxide melt grown eutectics have been proposed as an alternative to these dispersed electrodes,[4–6] based on its textured fine microstructure. In this case the porous metallic phase should be constrained between the narrow space left by the ionic conductive phase lamellae, which may hinder grain growth.

Several years ago, Revcolevschi et al. produced crystallographically aligned metal-oxide cermets by reduction of directionally solidified oxide eutectics.[7,8] In particular, they studied the kinetics of the reduction of NiO to metallic Ni in NiO-CaSZ (calcia-stabilized zirconia) oxide–oxide eutectics at 1075 °C under CO/CO_2 atmosphere.[9] The authors also suggested the existence of an electrochemical local cell process where the oxygen ion diffusion to the surface proceeds

* Corresponding author. Tel.: +34 976 761333; fax: +34 976 761229.
E-mail address: orera@unizar.es (V.M. Orera).

0955-2219/$ – see front matter © 2005 Elsevier Ltd. All rights reserved.
doi:10.1016/j.jeurceramsoc.2005.01.025

via the cubic zirconia electrolyte lamellae and the electrons through the conducting metallic Ni phase. The final product was a composite of dense Ni and CaSZ alternating lamellae. The large volume reduction of about 40% resulting from the NiO to Ni transformation was accommodated by large cracks in well-oriented and massive samples, which degrades the mechanical properties of the cermet.

Recently, we have reported on the production of lamellar Ni-CaSZ porous cermet plates by surface laser melting and directional solidification of NiO-CaSZ structured eutectic ceramics.[10] Chemical reduction treatments in H_2 atmosphere transformed the NiO into porous metallic Ni. In the present paper we report on the fabrication of CoO and NiO-YSZ eutectic oxides by the laser floating zone technique. We have studied the influence of the composition and solidification parameters in the eutectic microstructure. The transformation of the oxide–oxide eutectics into porous cermets has been done at different temperatures between 600 and 900 °C to ascertain which is the reduction mechanism that controls this process. For this study, we have chosen monolithic and homogeneous directionally solidified eutectic rod samples. The best processing conditions to obtain fine, thermally and mechanically stable, homogeneous porous cermets with controlled microstructures, as well as their electrical conductivity have been determined.

Moreover, it is known that some amount of Ni and Co can be dissolved into the YSZ phase during processing. This may significantly reduce the ionic conduction of the cermet and, in fact, the formation of tetragonal zirconia precipitates has been reported.[11] The clean YSZ skeleton, which has been analyzed in order to determine the properties of the matrix, was isolated by chemical removing the metal phase.

2. Experimental

NiO (Aldrich, 99.99%), CoO (Aldrich, 99.99%), ZrO_2 (Alfa, 99.9%) and Y_2O_3 (Aldrich, 99.99%) powders were milled, calcined, mixed and pressed. Rods, 2 mm in diameter and 50 to 100 mm in length, were prepared from a mixture of the oxide powders by pressureless sintering during 12 h at 1300 °C and 0.5 h at 1500 °C. Directionally solidified eutectic rods were produced from the precursor ceramic cylinders with a CO_2 continuous wave laser using the floating zone-method, as described elsewhere.[12,13] The thermal gradient at the growth front was about $G = 6 \times 10^5$ °C/m. Samples were isothermally and isochronally treated in a 4% H_2–N_2 gas mixture at temperatures from 600 to 900 °C in a tubular furnace. Progress of the reduction process was followed by gravimetric methods. The metallic phase was removed from reduced samples by reaction with diluted HNO_3 to obtain a porous, mechanically stable, YSZ lamellar skeleton.

The microstructure of the samples was studied by Optical Microscopy (OM) and Scanning Electron Microscopy (SEM). SEM micrographs and electron probe microanalysis (EPMA) were carried out with a JEOL 6400 microscope equipped with a Link Analytical eXL analyzer. Optical diffuse reflectance spectra were measured using a Praying Mantis Accessory for a Cary 500 spectrophotometer (Varian) and $BaSO_4$ as a standard. The conductivity measurements were performed using the four-point configuration at RT using a 220 Keithley Programmable current source and a Hewlett Packard 34401A microvoltmeter. Thermal expansion coefficients were measured within the 20 to 900 °C range using a Mettler TMA 40 dilatometer. Chemical composition of the YSZ phase was obtained by Energy Dispersive Spectroscopy (EDS) microanalysis using a Link Analytical analyzer fitted to a JEOL 2000 FXII Transmission Electron Microscope. For these experiments the Cliff-Lorimer method was employed,[14] where the Cliff-Lorimer sensitivity factors were experimentally measured from appropriate compound standards.

3. Experimental results and discussion

3.1. Microstructure and composition

The microstructure and composition of the samples play a crucial role in determining their suitability from the point of view of applications. For example, in Figs. 1 and 2 we illustrate three frequently encountered limitations. In Fig. 1 we show the microstructure of a well-ordered lamellae sample after reduction. As it can be seen, dense instead of porous metallic lamellae are obtained. Besides, the enormous strains resulting from the volume change taking place during the NiO to Ni reduction are accommodated by large longitudinal cracks as previously observed by Bonvalot-Dubois et al.[9]

It is also well known that rods grown from the melt tend to crack for large rod diameter values.[15] As shown in Fig. 2 (left), those cracks not only deteriorate the mechanical

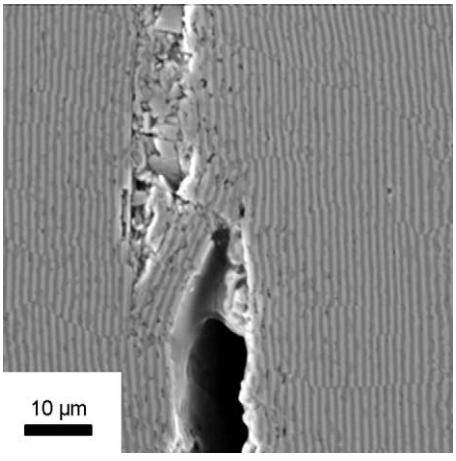

Fig. 1. SEM micrograph of a transverse cross section for a completely reduced Ni-YSZ cermet showing the residual stress accommodation cracks produced during reduction. (Brightness scale: light phase: Ni, dark: YSZ, black: pore.)

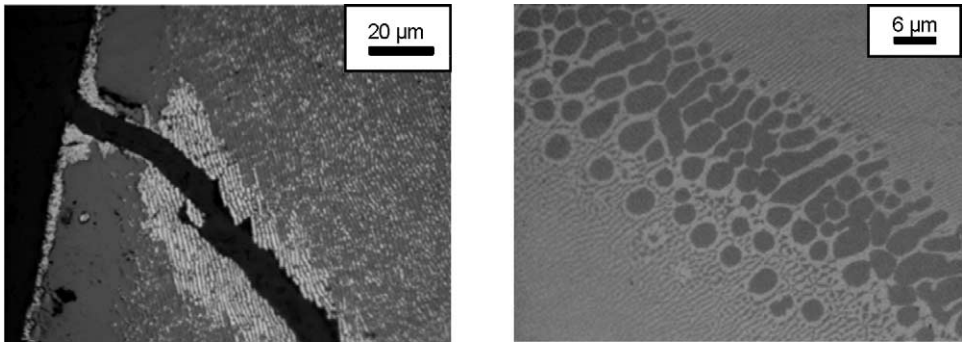

Fig. 2. Optical micrographs of transverse cross sections showing (left) a not fully reduced cermet with a crack produced during growth and (right) a non-reduced sample with YSZ primary phase. (Brightness scale: light phase: Ni, medium: NiO, dark: YSZ, black: pore.)

strength of the rod but they also seriously disturb the reduction process. Another matter of concern is the presence of primary phases if the composition of the eutectic is not well adjusted (see Fig. 2, right).

We are looking for samples with a very fine eutectic microstructure (lamellae thickness of 1 μm or less), without cracks and able to support the large strains associated with the reduction processes. We observed that severe cracking due to reduction (Fig. 1) could be eliminated if large aligned microstructures are avoided. We have varied the growth parameters and sample composition in order to achieve the optimal sample quality (homogeneous eutectic microstructure, absence of cracks and no segregation of primary phase). Oxidation of CoO to Co_2O_3 is avoided by growing in an Ar atmosphere. The best growth conditions to produce a fine and homogeneous microstructure are pulling speeds of $R = 100$ mm/h, a counter rotation of precursor and sample of 10 rpm, and laser powers of about 40 W during growth. Rod diameters must be less than 1.5 mm to avoid cracks. In terms of the G/R parameter that better describes the condition of the eutectic growth, we obtain $G/R = 2 \times 10^{10}$ °C s/m^2. The selected composition of the precursor ceramics are (mol%): 75 NiO–23.1 ZrO_2–1.9 Y_2O_3 and 80 CoO–18.5 ZrO_2–1.5 Y_2O_3, leading to a homogeneous eutectic microstructure.

This eutectic lamellar microstructure (Fig. 3) consists of 20–80 μm size eutectic grains with NiO (or CoO) lamellae (≈0.5 μm thickness) alternating with YSZ lamellae (≈0.4 μm). The interlamellar spacing ($\lambda \approx 0.9$) is compatible with the empirical relationship rate $\lambda^2 R = 10^{-4}$ mm^3/h, given by Dhalenne and Revcolevschi.[16] We analyzed the final composition of the eutectic samples by 2D image analysis. The results in vol% are: 56.5 ± 1.7 NiO–43.5 ± 1.7 YSZ and 61.0 ± 1.5 CoO–39.0 ± 1.5 YSZ, respectively. The content of the calculated transition metal oxide by this method is lower than the precursor composition, due to the solubility of transition metal oxide in the YSZ, as we will confirm in a further section.

3.2. Reduced samples

Reduction was done at temperatures above 600 °C. The composition of the resulting material has been determined by X-ray powder diffraction, indicating that all the transition metal oxide is fully transformed into metal and pores. Since the external dimensions of the sample do not change during the reduction process and cracks are not observed, we can obtain the final composition of the samples according to the results obtained by image analysis of the non-reduced samples. It corresponds in vol% to: 43.5 ± 1.7 YSZ–33.1 ± 1.0 Ni–23.4 ± 0.7 pores and 39.0 ± 1.5 YSZ–34.8 ± 0.9 Co–26.2 ± 0.6 pores, respectively. After reduction, the YSZ matrix remains apparently intact. There is no microstructure evolution at least during 40 h of reduction and temperatures up to 1200 K. Note that

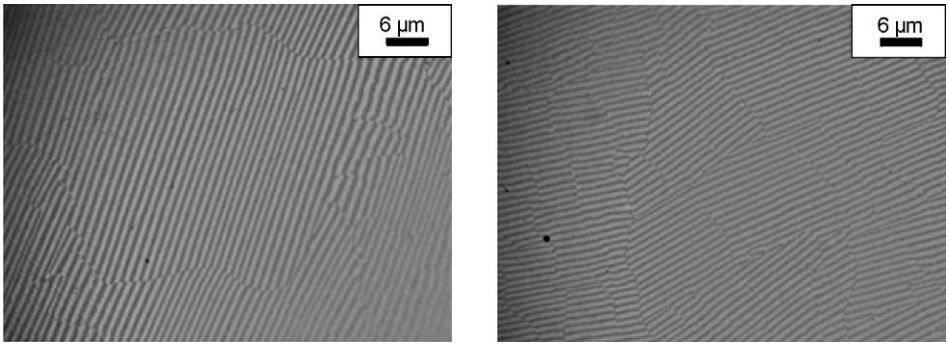

Fig. 3. Optical micrographs of transverse sections for (left) NiO-YSZ and (right) CoO-YSZ eutectics. (Brightness scale: light phase: NiO or CoO, dark: YSZ.)

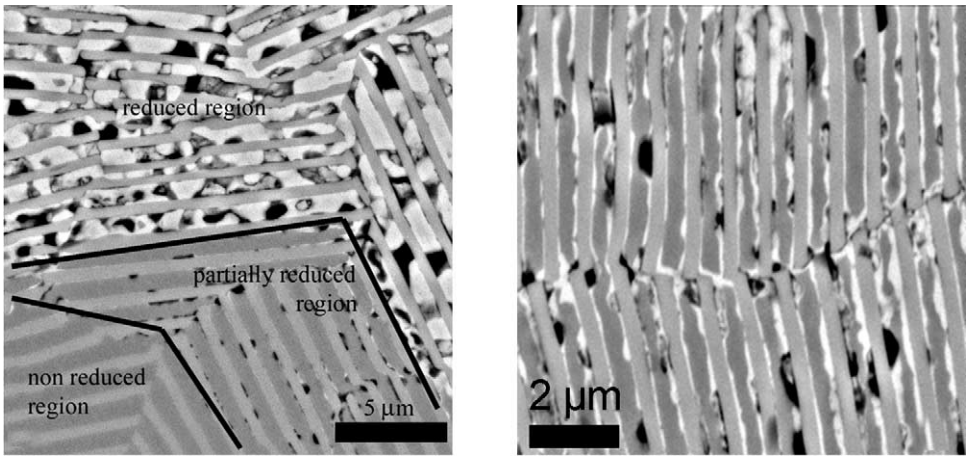

Fig. 4. SEM micrographs of transverse cross sections of a CoO-YSZ rod. Left: interface between reduced and non-reduced regions and (right) partially reduced region. (Brightness scale: light phase: Co, light grey: YSZ, dark grey: CoO, black: pore.)

the resulting materials consist of ≈41% porous Ni or ≈43% porous Co metal plates between the YSZ lamellae, and that alignment of the structure along the growth direction assures a good connection between phases.

In order to get some insight on the reduction process of the oxide–oxide eutectics some not fully reduced samples were analysed by SEM. The reduction mechanism is complex. As shown in Fig. 4, two limiting situations of the reduction front in cobalt–zirconia samples can be observed. The reduction front propagates faster when it is parallel, rather than perpendicular, to the lamellae (left). This is a consequence of the YSZ phase being an excellent oxygen ionic conductor. The oxygen ions leave the CoO towards the YSZ lamellae and diffuse easily along the YSZ lamellae to the external surface. The electrons required to maintain electronegativity move most likely along percolating Co particles, as illustrated in Fig. 4 (right). In our samples this anisotropic behaviour is averaged out in transverse cross sections by the grain structure. A similar mechanism for the Ni-YSZ cermet was observed.

Transverse cross sections of two samples, after complete reduction, are shown in Fig. 5. A homogeneous distribution of metal particles and pores is formed. They are confined by the zirconia skeleton that serves as a barrier against coarsening of the metallic particles.

The YSZ skeleton determines the thermomechanical behaviour of the porous cermet. In fact, we have measured the thermal expansion coefficients (within the 20–900 °C range), which are: $10.8 \times 10^{-6}\,K^{-1}$ for the Ni-cermet and $10.7 \times 10^{-6}\,K^{-1}$ for the Co-cermet. Both are very similar to that of the 8YSZ skeleton ($10.8 \times 10^{-6}\,K^{-1}$). Notice that this is a very important property to achieve good thermomechanical integration with the YSZ electrolyte.

3.3. YSZ skeleton

We characterized the YSZ phase as follows. After total reduction, all the transition metal phase was removed by reaction with diluted nitric acid thus obtaining the isolated YSZ matrix. X-ray diffraction experiments (Fig. 6) reveal only the cubic phase of the YSZ in both cermets (space group: $Fm\bar{3}m$), indicating that all the metal has been removed. From Rietveld refinements, we obtained the lattice parame-

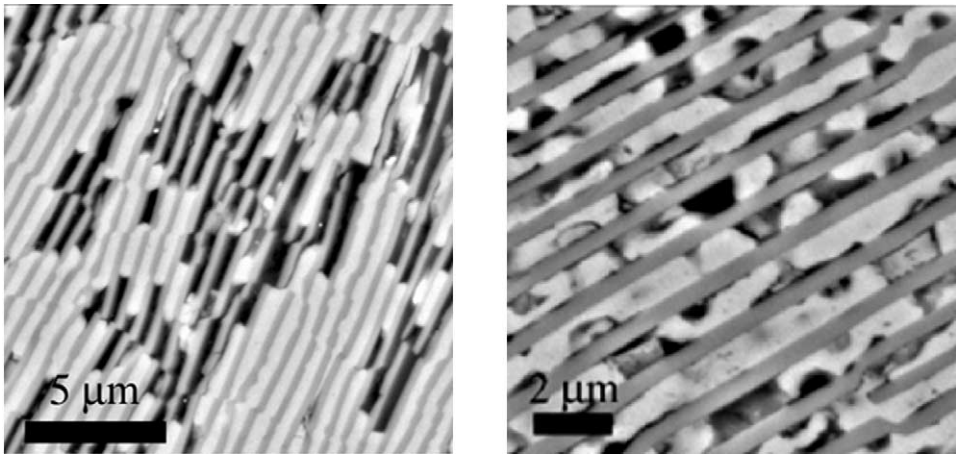

Fig. 5. SEM micrographs of transverse cross sections of completely reduced cermets of (left) Ni-YSZ and (right) Co-YSZ.

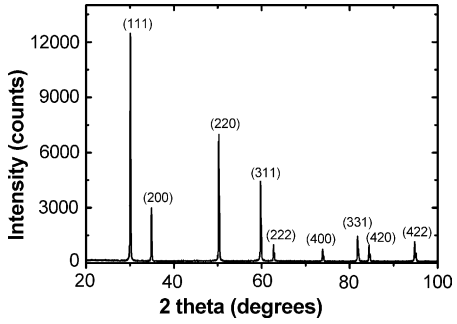

Fig. 6. X-ray powder diffraction spectrum of the cermet Co-YSZ after removal of the metal showing the diffraction peaks of the YSZ cubic lattice.

ters for the Ni-YSZ (5.127 ± 0.001 Å) and for the Co-YSZ sample (5.128 ± 0.001 Å), the same as was found by Ingel in 8YSZ.[17]

It is worthwhile keep in mind that the emptied YSZ skeleton, although fragile, has enough mechanical resistance to be handled. The amount of NiO and CoO dissolved in the reduced YSZ matrix was quantified by EDS microanalysis in the TEM. In this way, spurious signals coming from the transition metal lamellae that could be activated by bremsstrahlung X-rays produced in the TEM condenser aperture are avoided.[18] The results given in Table 1 correspond to the solubility of the transition metal in 8YSZ at the eutectic temperature (≈1850 °C).

Notice that Co solubility in YSZ is larger than Ni. The latter coincides with that given by Linderoth et al. in their study of the effect of NiO-Ni transformation in the 8YSZ matrix.[11] However, these authors reported a decrease of the YSZ lattice parameter with the Ni content, which we did not observe. NiO (or CoO) dissolved in the YSZ produces an increment in charge to compensate for oxygen vacancies. The final composition for the YSZ matrix is $Zr_{0.83}Y_{0.15}Ni_{0.02}O_{1.91}$ and $Zr_{0.80}Y_{0.15}Co_{0.05}O_{1.88}$, respectively. These samples would contain the same amount of oxygen vacancies as YSZ with 10 and 12 mol% of Y_2O_3 for the Ni and Co compounds, respectively.

Table 1
Composition of the YSZ phase in the cermets

Cermet	Y_2O_3 (mol%)	NiO or CoO (mol%)
Ni-YSZ	7.45 ± 0.12	1.99 ± 0.06
Co-YSZ	7.44 ± 0.31	4.95 ± 0.26

In order to determine whether the transition metal impurity was diluted to the atomic scale in the YSZ matrix or not, and also to get an insight of the impurity ion environment, we performed a spectroscopic study using the diffuse reflectance of the "emptied" samples. In both cases the optical properties correspond to the presence of transition metal oxide dissolved in the YSZ matrix. In Fig. 7 we compare the measured diffuse reflectance (transformed to absorbance) with the optical absorption spectra measured for single crystals of YSZ grown by the skull method and slightly doped with Ni(II) and Co(II). For the cobalt sample, the diffuse reflectance spectrum measured at 300 K reveals an intense triplet (centred at 557 nm), assigned to the transition $^4T_1$ (F) → $^4T_1$ (P), and another band (1277 nm) assigned to the transition $^4T_1$ (F) → $^4T_2$ (F), according to an octahedral crystal field for Co^{2+}. These results are in agreement with the absorption spectra measured at 300 K for the single crystal of YSZ:Co and with the previous work of Aleksandrov et al.[19]

The diffuse reflectance spectra measured for the Ni sample gives two bands at 423 and 525 nm. These bands were assigned, according to the work of Kunz et al.,[20] to the transitions $^3A_2$ (F) → $^3T_1$ (P) and $^3A_2$ (F) → $^1T_2$ (D), respectively. Similar results were obtained for the measured absorption spectra of the YSZ:Ni single crystal, giving also an octahedral crystal field for the Ni^{2+}.

3.4. Reaction kinetics during the reduction process

The reduction kinetics have been studied by monitoring the weight losses during isothermal reduction experiments given by M_t/M_∞ (the ratio between the actual mass loss and the loss when the sample is totally reduced) as a function of time (Fig. 8). Cylindrical samples of approximately the same size were partially reduced at different temperatures, then quenched to room temperature, weighed, and placed back into the furnace until transition metal oxide reduction was completed. This weight loss is due to the reduction of the transition metal oxide to the metal and agreed with the amount of transition metal oxide phase.

Isochronal experiments (Fig. 9), where the weight losses were measured for a given period of time at different temper-

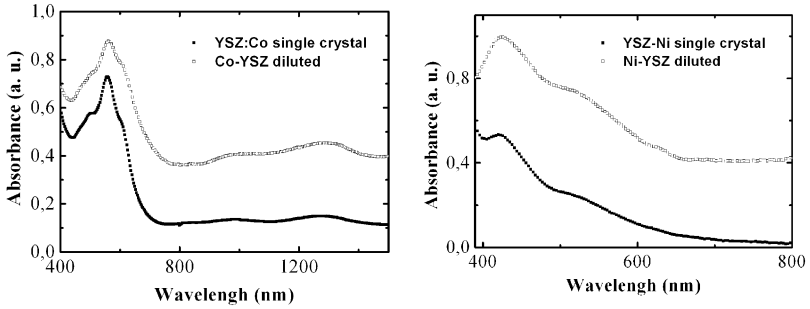

Fig. 7. Absorption spectra of (left) Co-YSZ and (right) Ni-YSZ measured at 300 K.

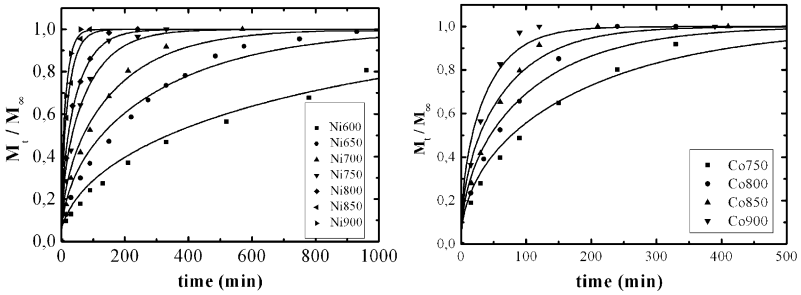

Fig. 8. Mass reduction fraction vs. time of (left) Ni-YSZ and (right) Co-YSZ samples. Experimental points and fitting curves using Eq. (6). In the insets, temperatures are in °C.

atures, show that for the Ni-YSZ cermet the reduction process is clearly temperature activated within the complete temperature range explored (600–900 °C). In the case of the Co-YSZ cermet, this is not so clear. As shown in Fig. 9, reduction at 600–700 °C occurs faster than at 750 °C.

The study of the progression of the reduction front reported in Section 3.2, indicates that the reduction takes place via a diffusion-limited process. This means that the kinetics of the reduction reaction

$$\mathrm{MO} + \mathrm{H_2} \rightarrow \mathrm{M} + \mathrm{H_2O(g)}, \mathrm{M} = \mathrm{Ni}, \mathrm{Co} \quad (1)$$

could be dominated by the diffusion of the same species, presumably that of oxygen ions through the YSZ matrix. The electrons are easily transported by the metallic phase.

However, for the cobalt samples a different mechanism seems to dominate at low temperatures. A possible explanation could be the competition between oxygen diffusion through the zirconia matrix and the pores. The oxygen diffusion rate through the zirconia decreases with decreasing temperature[21] and at low temperatures the diffusion through pores could compete. Besides, the gas flow through pores in the laminar regime decreases with increasing T,[22] which could explain the T-dependence observed for cobalt samples at the lowest reduction temperatures. Nevertheless, it is not yet clear why we only observe this competition for the Co-YSZ composites. Studies to clarify this behaviour are under way.

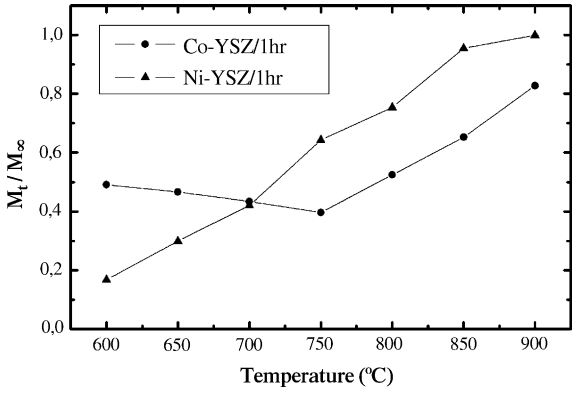

Fig. 9. Reduced fraction M_t/M_∞ vs. T (°C) after 1 h of reduction for the NiO-YSZ and CoO-YSZ samples.

We now analyse the kinetic curves in the thermally activated range, given in Fig. 8. The mathematical theory of diffusion in isotropic substances is based on the hypothesis that the rate of transfer of the diffusing substance through a unit area of section is proportional to the concentration gradient measured normal to the section, according to Fick's Law:

$$\vec{F} = -D\vec{\nabla}C \quad (2)$$

where F is the flux of the diffusing substance, C is the concentration, and D is the effective diffusion coefficient.

If the diffusion coefficient is constant and for an infinite cylinder of radius a with a constant surface concentration of diffusing species C_0 the solution for Eq. (2) is[23]

$$\frac{C(r,t) - C_1}{C_0 - C_1} = 1 - \frac{2}{a}\sum_{n=1}^{\infty} \frac{\exp(-D\alpha_n^2 t) J_0(r\alpha_n)}{\alpha_n J_1(a\alpha_n)} \quad (3)$$

where $J_i(x)$ are the Bessel function of the first kind, C_1 is the initial concentration inside the cylinder, and $a\alpha_n$ are the positive roots of $J_0(x)$. In terms of the measured M_t/M_∞ quotient this equation can be transformed into:

$$\frac{M_t}{M_\infty} = 1 - \sum_{n=1}^{\infty} \frac{4}{a^2\alpha_n^2} \exp(-D\alpha_n^2 t) \quad (4)$$

In Fig. 8 we plot the results of the isothermal reduction studies performed in Ni-YSZ and Co-YSZ samples. We used long enough samples (≈6 mm) compared with the diameter (≈1.4 mm) to use Eq. (4). The experimental data are well described by this equation leaving as a fitting parameter the effective diffusion coefficient D.

Table 2
Effective diffusion coefficients for NiO-YSZ and CoO-YSZ systems in the range of temperatures studied

Temperature (°C)	D_{eff} (cm^2/s) NiO-YSZ	D_{eff} (cm^2/s) CoO-YSZ
600	1.8×10^{-8}	–
650	5×10^{-8}	–
700	9.1×10^{-8}	–
750	1.9×10^{-7}	1.1×10^{-7}
800	3×10^{-7}	1.9×10^{-7}
850	6.3×10^{-7}	3×10^{-7}
900	9.8×10^{-7}	5×10^{-7}

Effective diffusion coefficients for both compounds are shown in Table 2. It is important to notice that the value of the effective diffusion coefficient is higher in the Ni-YSZ sample (by a factor of 2, approximately). This is in part due to the higher volumetric fraction of the YSZ in the Ni-YSZ cermet and also, in part because of the lower oxygen vacancy concentration in Ni-samples (due to the lower content of transition metal oxide dissolved in the YSZ) that increases the oxide ion conductivity, as we will discuss in the next section. The diffusion coefficients for Ni-YSZ samples follow an Arrhenius type law

$$D(T) = D_0 \exp\left(-\frac{E_a}{kT}\right) \quad (5)$$

In Fig. 10 the effective diffusion values, which control the thermally activated reduction process in NiO-YSZ, are compared with the oxygen diffusion coefficient obtained from conductivity measurements for YSZ (10 mol% Y_2O_3, single-crystal).[21] The comparison corroborates that the diffusive species in the NiO-YSZ eutectic (and also for the CoO-YSZ at high temperatures) is very likely the oxygen ion. The oxygen readily diffuses through the eutectic matrix, 5 to 10 times faster than in bulk YSZ. This is probably a consequence of oxygen diffusing through a combination of oxide ions along YSZ and O_2 gas along pores. The value for the activation energy (E_a = 1.16 eV for the NiO-YSZ) is also a little higher than in pure 10YSZ (E_a = 1.04 eV). We believe that this increase in the activation energy in the YSZ can be caused by the presence of the transition metal ion impurities dissolved into the YSZ matrix and their associated charge compensating oxygen ion vacancies. This increase in the oxygen vacancy concentration lowers the diffusion coefficient and increases the activation energy in cubic YSZ beyond the optimum vacancy concentration corresponding to the 8YSZ composition.[24]

3.5. Conductivity measurements

The actual ionic YSZ conductivity in the eutectics cannot be measured directly. The electrical conductivity of the composite is dominated by the transition metal oxide in as-grown conditions, which are semiconducting and several orders of magnitude better conductors than YSZ, and by the metal in the reduced cases.[7] The electronic conduction in the cermet is also an important parameter if it is to be used as anode for current collection in a solid-oxide fuel cell. We have measured the conductivity at RT in some reduced samples using the dc four-point technique. In these experiments, a current of 100 mA flows along the growth direction. The observed resistivity (mean value ± standard deviation) are 54 ± 16 μΩ cm for Co-YSZ and 172 ± 50 μΩ cm for Ni-YSZ. These values are to be compared with the bulk resistivity of the corresponding metals, 6.24 μΩ cm for cobalt and 6.84 μΩ cm for nickel.[25] The resistivity is around nine times larger in the Co-YSZ cermet than in metallic Co, and the ratio increases in the case of the Ni-YSZ cermet ($\rho_{Cermet}/\rho_{Nickel}$ = 25). The resistivity ratio is always larger in Ni-YSZ than in Co-YSZ. The larger volume fraction occupied by Co in the Co-YSZ cermet than by Ni in the Ni-YSZ cermet (34.8 and 33.1% as estimated in Section 3.2), can contribute to this effect. The second fact that could give rise to this difference between both cermets may have its origin in the differences in metallic particle connectivity. However, until now the two-dimensional SEM micrographs used to investigate the microstructure of the cermets do not give conclusive information on this matter. In addition, it is important to note that the measured resistivity values in Ni-YSZ are lower by a factor of 2 than in well conducting isotropic cermets reported in the literature,[26,27] a consequence of the aligned nature of our cermets, which are strongly textured along the growth direction.

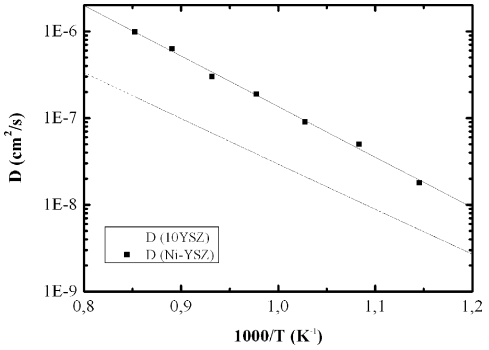

Fig. 10. $D(T)$ vs. $1/T$ for 10YSZ (E_a = 1.04 eV)[21] and NiO-YSZ (E_a = 1.16 eV, this work).

4. Conclusions

We have produced dense and free of cracks rods of NiO-YSZ and CoO-YSZ eutectics by the LFZ method. Growth rate, composition and diameter have been adjusted to achieve a homogeneous eutectic microstructure with interface spacing around 1 μm. These eutectic rods have been used to study the reduction process of NiO to Ni and CoO to Co. The transition metal oxide is transformed to porous metal during reduction, producing a porous microstructured cermet consisting of alternate porous lamellae of Ni (or Co) (electronic conductor) sustained by the YSZ skeleton (ionic conductor). Diffusion of the O^{2-} ions takes place preferentially along the YSZ phase with activation energies slightly larger than for pure 8YSZ, owing to the presence of Ni^{2+} and Co^{2+} doping ions.

The electrical resistivity of the reduced eutectics is smaller (by a factor of 2), compared with other isotropic cermets reported in the literature. Thermoelastic properties of the cermet are dominated by the YSZ skeleton, which make the material very promising as an anode substrate for YSZ thin film electrodes.

Acknowledgements

M.A. Laguna-Bercero is a Ph.D. Student of CSIC (I3P Program) financed by the European Social Fund. We thank

the CICYT (MAT2000-1495 and MAT2003-01182) for financial support and Dr. Jolanta Stankiewicz for her help in conductivity measurements.

References

1. Lee, J. H., Heo, J. W., Lee, D. S., Kim, J., Kim, G. H., Lee, H. W. *et al.*, The impact of anode microstructure on power generating characteristics of SOFC. *Solid State Ionics*, 2003, **158**, 225–232.
2. Markin, T. L., Bones, R. J. and Dell, R. M., High temperature solid electrolyte fuel cells. In *Proceedings of a Conference of Superionic Conductors*. Plenum Press, New York, 1976, pp. 15–35.
3. Minh, N. Q., Ceramic fuel cells. *J. Am. Ceram. Soc.*, 1993, **76**(3), 563–588.
4. Gerk, C. and Willert-Porada, M., Application of eutectic ceramic mixtures for the functional components of high temperature SOFCs. In *9th CIMTEC 98, Innovative Materials in Advanced Energy Technologies*, 1999.
5. Orera, V. M., Peña, J. I., Merino, R. I., Larrea, A. and De la Fuente, G. F., *10th International Ceramics Congress, CIMTEC 2002*, ed. P. Vincenzini. *Advances in Science and Technology, Vol 30*. Techna, Faenza, 2003, pp. 885–896.
6. Garcia, G., Merino, R. I., Orera, V. M., Larrea, A., Peña, J. I., Laguna-Bercero, M. A. *et al.*, YSZ thin films deposited on NiO-CSZ anodes by PIMOCVD for IT-SOFC. *Adv. Mater. Chem. Vap. Deposit.*, 2004, **10**, 249–252.
7. Revcolevschi, A. and Dhalenne, G., Crystallographically aligned metal-oxide composite made by reduction of directionally solidified oxide–oxide eutectics. *Nature*, 1985, **316**, 335–336.
8. Revcolevschi, A. and Dhalenne, G., Engineering oxide–oxide and metal–oxide microstructures in directionally solidified eutectics. *Adv. Mater.*, 1993, **9**, 657–662.
9. Bonvalot-Dubois, B., Dhalenne, G., Berthon, J., Revcolevschi, A. and Rapp, R. A., Reduction of NiO platelets in a NiO/ZrO_2(CaO) directional composite. *J. Am. Ceram. Soc.*, 1988, **71**, 296–301.
10. Merino, R. I., Peña, J. I., Laguna-Bercero, M. A., Larrea, A. and Orera, V. M., Directionally solidified calcia stabilised zirconia–nickel oxide plates in anode supported SOFC's. *J. Eur. Ceram. Soc.*, 2004, **24**, 1349–1353.
11. Linderoth, S., Bonanos, N., Jensen, K. V. and Bilde-Sorensen, J. B., Effect of NiO-to-Ni transformation on conductivity of yttria-stabilized ZrO_2. *J. Am. Ceram. Soc.*, 2001, **84**, 2652–2656.
12. de la Fuente, G. F., Díez, J. C., Angurel, L. A., Peña, J. I., Sotelo, A. and Navarro, R., Wavelength dependence in laser floating zone processing. A case study with Bi–Sr–Ca–Cu–O superconductors. *Adv. Mater.*, 1995, **7**, 853–856.
13. Peña, J. I., Merino, R. I., de la Fuente, G. F. and Orera, V. M., Aligned ZrO_2(c)–$CaZrO_3$ eutectics grown by the laser floating zone method: electrical and optical properties. *Adv. Mater.*, 1996, **8**, 909–912.
14. Cliff, G. and Lorimer, G. W., The quantitative analysis of thin specimens. *J. Microsc.*, 1975, **103**, 203–207.
15. Peña, J. I., Merino, R. I., Harlan, N. R., Larrea, A., de la Fuente, G. F. and Orera, V. M., Microstructure of Y_2O_3 doped Al_2O_3–ZrO_2 eutectics grown by the laser floating zone method. *J. Eur. Ceram. Soc.*, 2002, **22**, 2595–2602.
16. Dhalenne, G. and Revcolevschi, A., Directional solidification in the NiO–ZrO_2 system. *J. Cryst. Growth*, 1984, **69**, 616–618.
17. Ingel, R. P. and Lewis III, D., Lattice parameters and density for Y_2O_3-stabiliced ZrO_2. *J. Am. Ceram. Soc.*, 1986, **69**(4), 325–332.
18. Williams, D. B. and Carter, C. B., *Transmission Electron Microscopy*. Plenum Press, New York, 1996.
19. Aleksandrov, V. I., Batygov, S. K h., Vishnyakova, M. A., Voron'ko, Yu. K., Kakabukhova, V. F., Lavrishchev, S. V. *et al.*, Influence of composition and heat treatment on charge states of intrinsic and impurity defects in ZrO_2–Y_2O_3 solid solutions. *Sov. Phys. Solid State*, 1984, **26**(5), 799–803.
20. Kunz, M., Kretschmann, H., Assmus, W. and Klingshirn, C., Absorption and emission spectra of yttria-stabilized zirconia and magnesium oxide. *J. Lumin.*, 1987, **37**, 123–131.
21. Casselton, R. E. W., Low field DC conduction in yttria-stabilized zirconia. *Phys. Stat. Sol. (a)*, 1970, **2**, 571–585.
22. Barrer, R. M., *Diffusion in and Through Solids*. University Press, Cambridge, 1941.
23. Crank, J., *The Mathematics of Diffusion* (*2nd ed.*). Clarendon Press, Oxford, 1975.
24. Subarao, E. C., Science and technology of zirconia. In *Advances in Ceramics*, *Vol 3*, ed. A. H. Heuer and L. W. Hobbs. The American Society, 1981, pp. 1–24.
25. *Handbook of Chemistry and Physics* (*55th ed.*). CRC Press, Inc., 1974.
26. Simwonis, D., Tietz, F. and Stöver, D., Nickel coarsening in annealed Ni/8YSZ anode substrates for solid oxide fuel cells. *Solid State Ion*, 2000, **132**, 241–251.
27. Skartmousos, D., Tsoga, A., Noumidis, A. and Nikolopoulos, P., 5 mol% TiO_2-doped Ni-YSZ anode cermets for solid oxide fuel cells. *Solid State Ion*, 2000, **135**, 439–444.